Journal of the Meteorological Society of Japan, Vol. 88, No. 3, pp. 395–407, 2010.
DOI:10.2151/jmsj.2010-308

Influence of the Maritime Continent on the Boreal Summer Intraseasonal Oscillation

Weijun ZHU

Key Laboratory of Meteorological Disaster of Ministry of Education, Nanjing University of Information Science & Technology, Nanjing, China
IPRC and Department of Meteorology, University of Hawaii, Honolulu, USA

Tim LI and Xiouhua FU

IPRC and Department of Meteorology, University of Hawaii, Honolulu, USA

Jing-Jia LUO

Climate Variations Research Program, Frontier Research Center for Global Change, JAMSTEC, Yokohama Japan

(Manuscript received 30 July 2009, in final form 26 February 2010)

Abstract

The effect of the Maritime Continent (MC) on the propagation characteristics of the boreal summer intraseasonal oscillation (ISO) over the Indo-western Pacific region were investigated by performing high-resolution (T159) atmospheric general circulation model (AGCM) simulations that remove and retain the MC. The most significant difference, as revealed by a finite domain wavenumber-frequency spectral analysis is the weakening of the northward propagation of ISO over the Asian monsoon region (65°–160°E) when the MC is removed; a less significant difference is the enhancement of the eastward propagation along the equator. The diagnosis of the vertical structure of the simulated ISO and the model mean flow indicates that the weakening of the northward propagation is primarily attributed to the reduction of the background easterly shear, low-level southerly and meridional humidity gradient, all of which contribute to the weakening of meridional asymmetries of vorticity and humidity fields with respect to the ISO convection center. The enhanced eastward propagation is possibly attributed to the strengthening of the mean convection over the MC in association with the increase of the local surface moisture and moist static energy.

1. Introduction

Since the discovery of the Madden-Julian Oscillation (MJO) (Madden and Julian 1971, 1972), numerous studies have been devoted to understanding the temporal-spatial pattern and dynamics of the intraseasonal oscillation (ISO). As one of the most significant signals in the tropics, ISO has remarkable seasonal and regional characteristics. The initiation of ISO in the western Indian Ocean is possibly caused by local boundary layer processes (Jiang and Li 2005), air-sea interactions (Li et al. 2008), the circumnavigation of a preexisting MJO along the equator (Lau and Peng 1987; Mathews 2008), and/or interactions with mid-latitude perturbations (Hsu et al. 1990; Pan and Li 2007). While MJO exhibits a pronounced eastward propagation along the equator in boreal winter with a pronounced planetary zonal scale (Li and Zhou 2009), the boreal summer ISO (BSISO) is dominated by northward propagation in the Asian monsoon sector (e.g., Yasunari 1979; Krishnamurti and Sabrahmanyam 1982; Chen and Murakami 1988). Various theories have been proposed to understand the northward propagation in monsoon regions. Web-

Corresponding author: Weijun Zhu, Key Laboratory of Meteorological Disaster of Ministry of Education, Nanjing University of Information Science & Technology, 219 Ningliu Road, Nanjing 210044, China.
E-mail: weijun@nuist.edu.cn

ster (1983) proposed a land-atmosphere interaction mechanism. Wang and Xie (1997) indicated that the northward propagation is associated with north-westward emanation of Rossby waves from the Maritime Continent. Jiang et al. (2004) proposed two internal atmospheric dynamics mechanisms, the vertical shear mechanism and the moisture-convection feedback mechanism. They suggested that the monsoon easterly vertical shear, the climatological mean surface southerly and meridional moisture gradient may result in a north-south asymmetry between the ISO convection and vorticity/moisture fields, leading to northward propagation.

Given the fact that the strongest northward bifurcation of BSISO appears west of Sumatra, a natural question is what is the role of the Maritime Continent in causing the northward propagation? Observations show that the BSISO convective activities are in general suppressed over the Maritime Continent. The possible factors that suppress the BSISO convection are 1) the relatively low specific humidity compared to the surrounding ocean regions, 2) larger momentum dissipation over the land, and 3) a pronounced diurnal cycle in the region in association with the land-sea distribution. (e.g., Salby and Hendon 1994; Wang and Li 1994; Zhang and Hendon 1997; Neale and Slingo 2003; Maloney and Sobel 2004; Inness and Slingo 2006).

In this study, we intend to address the question by examining the effect of the Maritime Continent on the BSISO using a high-resolution global atmospheric general circulation model (AGCM). By designing an idealized numerical experiment that removes the land effect of the Maritime Continent and comparing the simulation with the one that retains the Maritime Continent, we examine how the BSISO propagation characteristics change and what are the fundamental mechanisms responsible for such changes. The rest of this paper is organized as follows. The numerical experiments and analysis methods are described in Section 2. The major differences in the BSISO propagation between the two simulations are described in Section 3. The physical mechanisms responsible for the differences are discussed in Section 4. The results are summarized in Section 5.

2. Experiment design and analysis methods

2.1 Experimental framework

The model used in this study is the ECHAM AGCM version 5.3 (Roeckner et al. 2003). The horizontal resolution is T159 ($0.75^\circ \times 0.75^\circ$), and the top of the model level is 10 hPa. Such a high resolution enables us to resolve the Maritime Continent land effect. Liess et al. (2005) noted a general improvement of the ISO simulation with high horizontal resolution. The ECHAM5 utilizes a semi-Lagrangian advection scheme (Lin and Johnson 1996), a prognostic-statistical scheme for the total water content (Tompkins 2002), and a modified Tiedtke (1989) mass flux scheme for cumulus convection (Nordeng 1994). The model is forced by climatological annual cycle sea surface temperature (SST) and ice fields from the Atmospheric Model Intercomparison Project (AMIP2). The initial condition is rather arbitrary, taken from the European Center for Medium-range Weather Forecasting (ECMWF) analysis on January 1, 1978.

For the control experiment (CTL), the model is integrated for 11 years, and the last 10-years 6 hourly outputs are used for the analysis. To examine the role of the Maritime Continent on the ISO, a sensitivity experiment is designed in which the model parameters are kept the same as in the CTL except that the Maritime Continent is removed (see Fig. 1 for the model land-sea mask and orography). SST in the original Maritime Continent grid is interpolated from the surrounding ocean points. This simulation is referred to as the no-Maritime Continent experiment (NOMC).

2.2 Analysis methods

In this study, a finite domain of 40°E–140°W and 10°S–30°N is chosen to examine the zonal and meridional BSISO propagations. This limited domain is chosen because the rainfall anomalies associated with the eastward and northward propagating BSISO modes are primarily confined over the Asian-Pacific monsoon region. A wavenumber-frequency spectral (WFS) analysis is employed to transform the model precipitation rate field from a space-time domain to a wavenumber-frequency domain. Conventionally, spatial decomposition is carried out along a full longitudinal circle (e.g., Hayashi 1982). Teng and Wang (2003) extended this analysis from a global domain to a finite domain on the basis of the fact that the BSISO is effectively trapped in the northern summer monsoon region by the lower boundary conditions (such as SST and surface moisture distributions) and the three-dimensional monsoon mean flows (Wang and Xie 1997). In addition, the WFS analysis along a meridional finite domain was also performed to study

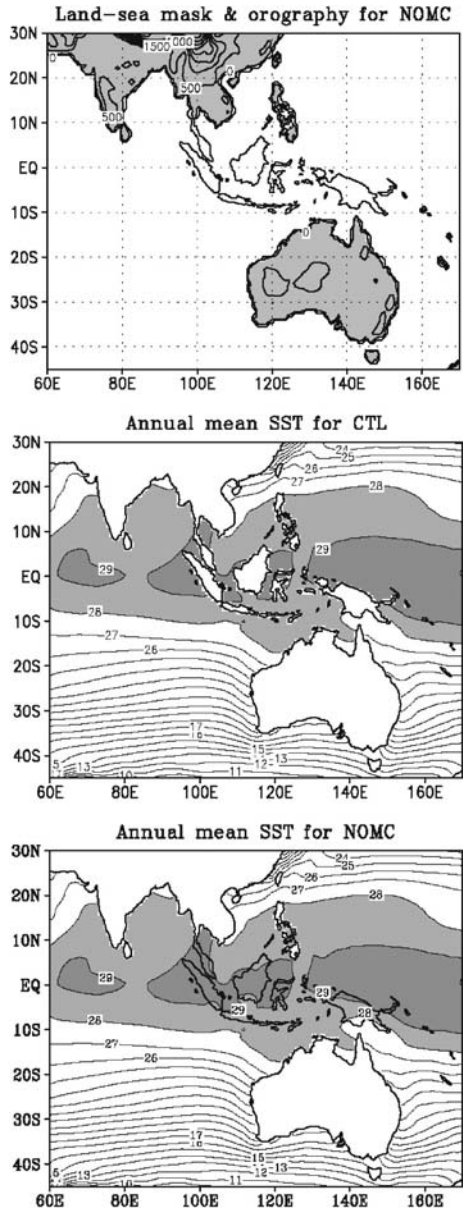

Fig. 1. The model land-sea mask (land shaded) and orography (thick black line, unit: m) specified in the no-Maritime Continent NOMC experiment (top panel) and the annual mean sea surface temperature SST fields specified in the control experiment CTL (middle panel) and NOMC (bottom panel) experiment (unit: °C).

the BSISO northward propagation (e.g., Teng and Wang 2003; Fu et al. 2003; Lin and Li 2008).

This regional WFS analysis is performed for each individual year from May 1 to October 31, and the spectrum at each summer is then averaged for the entire analysis period. The summer period in this study is from May to October (MJJASO).

A band-pass filtering scheme (Rui and Wang 1990) is applied to the observed and model variables to retain the intraseasonal (10–90-day) signal. First, an annual cycle is defined as the sum of the annual mean and the first three harmonics. The annual cycle is then subtracted from the original daily data to yield a daily anomaly.

To check the reliability of the model simulations, the NCEP-NCAR daily reanalysis and the CPC merged analysis of daily precipitation (CMAP, Xie and Arkin 1997) data obtained during 1979–1998 are used for comparison.

2.3 Model performance

Before examining the change in BSISO propagating features, we first examine the model performance in the simulation of the mean monsoon and intraseasonal variability. Figure 2a plots the observed (CMAP) and simulated (CTL and NOMC) climatological rainfall and 850-hPa winds in boreal summer. Compared to the observation (top panel), the simulation (bottom panels) captures the rainfall maxima over the Bay of Bengal, equatorial Indian Ocean, and western North Pacific (WNP). The rainfall centers in the eastern Arabian Sea and the South China Sea, which are usually not reproduced well in the lower version or coarser resolution of ECHAM AGCMs, are also to a large extent reproduced in the present model. The rainfall centers around Philippine and the South Pacific convergence zone (SPCZ); however, are slightly shifted northwestward. All the simulated rainfall maxima are to some degree overestimated, and the rainfall over the Maritime Content is substantially increased in NOMC than that in CTL. The most notable circulation features in boreal summer over the south Asian monsoon region are the cross-equatorial Somali jet and westerlies in the lower troposphere. These features are well reproduced by the ECHAM AGCM.

Figure 2b presents the observed (CMAP) and simulated (CTL and NOMC) standard deviation of the intraseasonal rainfall in boreal summer over the Asia–western Pacific sector. In the observations (top panel; also referred to Fu et al. 2003), there are five active regions of the BSISO: the eastern Arabian Sea, Bay of Bengal, equatorial Indian Ocean, South China Sea, and the WNP. In the CTL (middle panel) and NOMC (bottom panel) experiments,

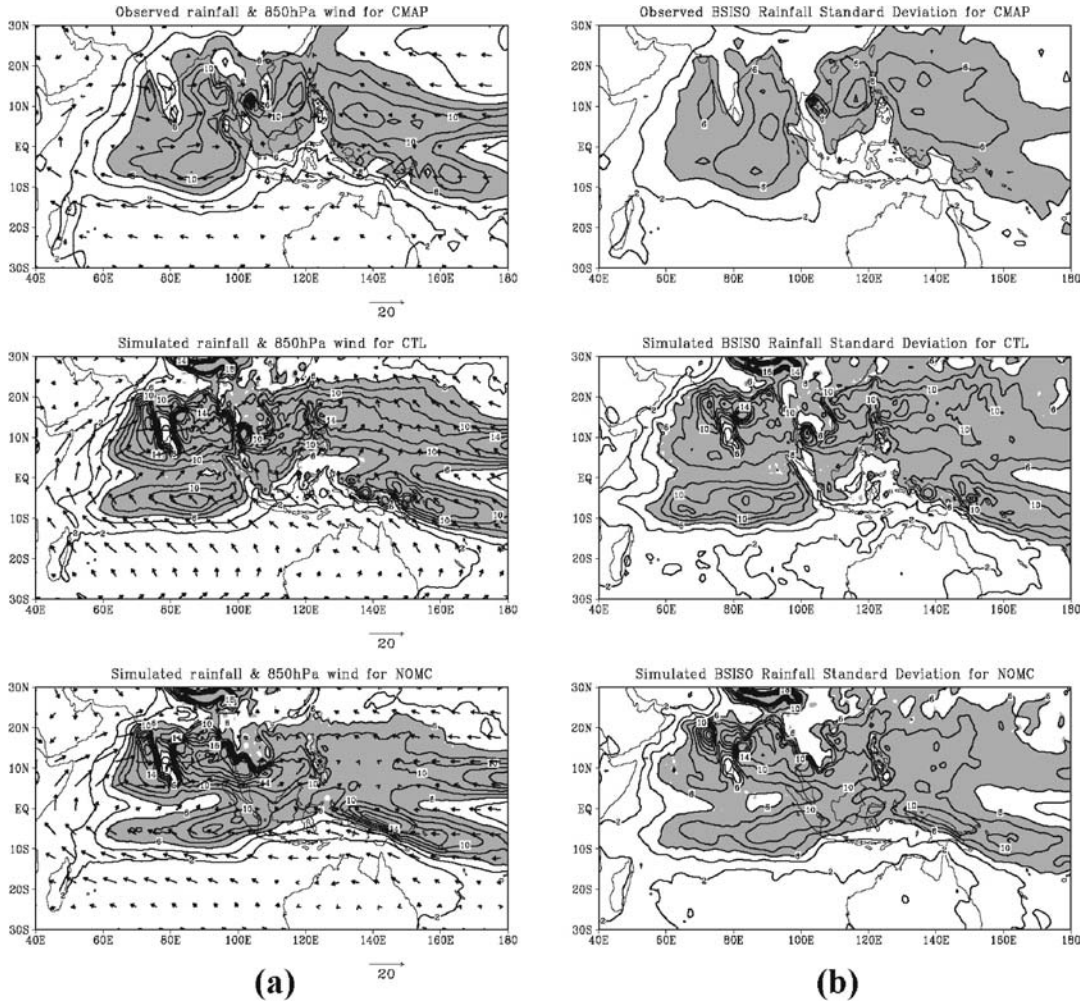

Fig. 2. (a) The climatological rainfall (mm day^{-1}) and 850-hPa winds (m s^{-1}) (left panels) and (b) the standard deviation of intraseasonal rainfall (mm day^{-1}) (right panels) during boreal summer calculated on the basis of the CPC merged analysis of daily precipitation CMAP observation (top panels), control CTL experiment (middle panels) and no-Maritime Continent NOMC experiment (bottom panels). Contour interval is 2 mm day^{-1}.

the five activity centers are well reproduced. The model, however, overestimates the strength of the BSISO activity considerably over the strong mean convection regions, and the area-averaged BSISO activity over the Maritime Content region (65°–160°E, 10°S–10°N) is greatly enhanced by 30% in NOMC compared with that in CTL.

3. Changes of BSISO propagation characteristics

The zonal propagation mode consists of both eastward and westward propagation. Firstly, we conduct the WFS analysis for the longitude domain of 40°E–140°W. Figure 3 shows the wavenumber-frequency distribution of variance of the zonal propagation mode averaged along 5°S–5°N on the basis of the rain rate fields from CMAP observation, CTL and NOMC, and their difference. In CTL, the most prominent eastward and westward propagation variances are primarily confined to the wavenumber 1 and the 30–50-day period, in good agreement with the CMAP observation (top panel) and previous observational analyses (e.g., Teng and Wang 2003; Lin and Li 2008). A weakness of the model is that it reproduces too symmetric eastward and westward propagations. When the Maritime Continent is removed, the eastward-propagating wavenumber-1 mode is enhanced, which can be clearly seen from the difference field (bottom

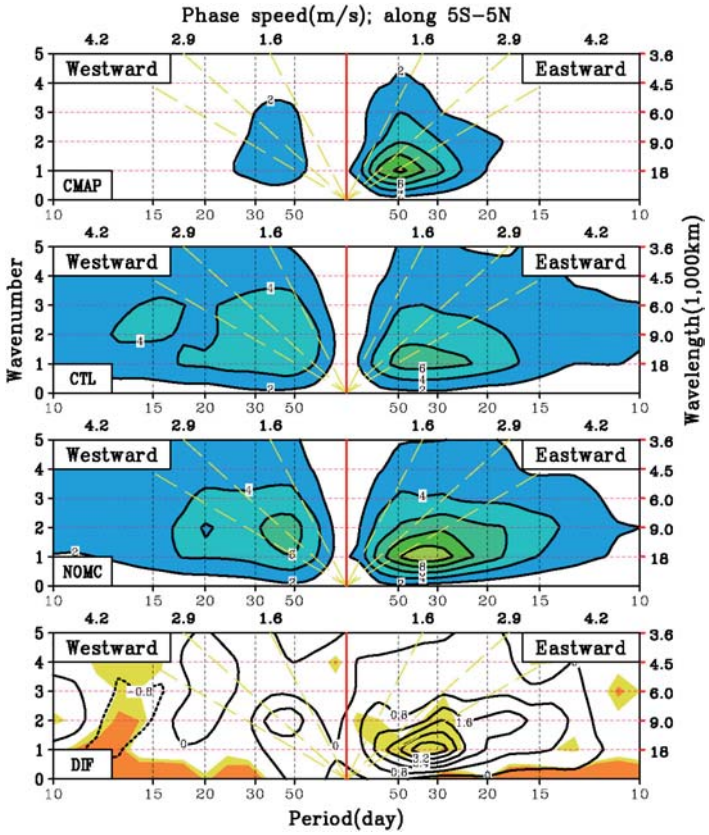

Fig. 3. The wavenumber-frequency spectrums for the zonal propagation mode averaged along 5°S–5°N calculated on the basis of the rain rate fields from the CPC merged analysis of precipitation CMAP observation, control CTL experiment, no-Maritime Continent NOMC experiment, and their difference (NOMC–CTL), respectively (from top to bottom panels). The contour interval for top three panels is 2.0 $(\text{mm day}^{-1})^2$ and is 0.8 $(\text{mm day}^{-1})^2$ for the bottom panels. Light (dark) yellow shaded areas in the bottom panel represent the significance level exceeding 90% (95%).

panel). However, such a difference does not exceed the 95% confidence level.

In contrast to the enhanced eastward propagation along the equator, the northward propagation of BSISO is weakened over the entire Asian monsoon domain. To focus on the northward BSISO propagation in the monsoon sector, we conducted a meridional wavenumber-frequency analysis between 10°S and 30°N, averaged for 10 boreal summers (from May to October, MJJASO) over the longitudinal domain of 65°–160°E. Figure 4 shows the wavenumber-frequency spectrum for the meridional propagating BSISO modes based on the rain rate fields in the CMAP observation, CTL, NOMC, and their difference. In CTL, the northward-propagating ISO variance is considerably greater than that of the southward-propagating mode. The maximum spectrum appears at the period of 30–50 days and the wavelength of 4,000 km. The corresponding northward phase propagation speed is about 1.2 ms^{-1}. The model simulation is consistent with the observation (top panel). The difference between the NOMC and the CTL runs indicates that removing the Maritime Continent results in a significant decrease of variance of the northward propagating ISO mode at a wide range of periods from 20 to 50 days. The maximum reduction of the ISO intensity is about 25% at the period of 30 days. The difference exceeds the 95% confidence level.

4. Cause of the changes in the BSISO propagation

4.1 Northward propagation

In this section, we investigate the physical mechanisms responsible for the changes in the BSISO propagation characteristics. Our focus is on the

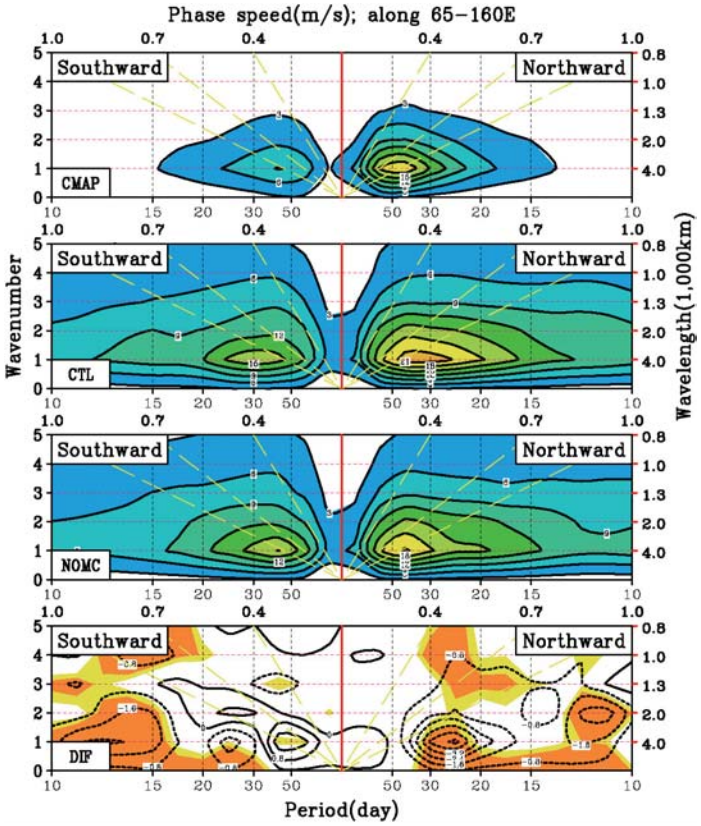

Fig. 4. Same as Fig. 3, but for the meridional propagation mode averaged along 65°–160°E.

two internal atmospheric dynamical mechanisms proposed by Jiang et al. (2004). The major dynamics associated with the vertical wind shear mechanism are the generation of the barotropic vorticity and divergence to the north of the ISO convection due to the barotropic and baroclinic mode coupling in the presence of the background easterly shear. The major process associated with the moisture-circulation feedback is the northward shift of the specific humidity relative to the convection center, owing to the moisture advection by the background southerly and the mean meridional humidity gradient.

Figure 5 illustrates the meridional-vertical structures of the composite northward-propagating BSISO mode from the CTL and NOMC simulations. The composite cases are selected following Jiang et al. (2004). Two objective criteria are applied to the filtered rainfall data averaged over 65°–160°E: 1) a positive rainfall anomaly continuously moves northward at least from the equator to 10°N; 2) in the course of the northward progression, the positive rainfall anomaly with amplitude greater than 5 mm day^{-1} must extend 10° or more in latitude. A reference time (day 0) is set when the northward propagating rainfall anomaly arrives at 5°N. According to the above criteria, 30 (16) strong northward propagation events are selected from the CTL (NOMC) simulation.

Figure 5 shows that the most striking asymmetry with respect to the ISO convection (represented by maximum rainfall) center appears in the vorticity field (top panels). A positive (negative) vorticity perturbation with an equivalent barotropic structure appears north (south) of the convection center, similar to the observation (see Jiang et al. 2004). While the asymmetric vorticity perturbation appears in both of the CTL and NOMC experiments, the intensity of the asymmetric vorticity is considerably reduced by 50% while the Maritime Continent is removed.

A further examination of the background mean vertical shear from the two experiments (Fig. 6a) confirms the vertical shear mechanism. The reduc-

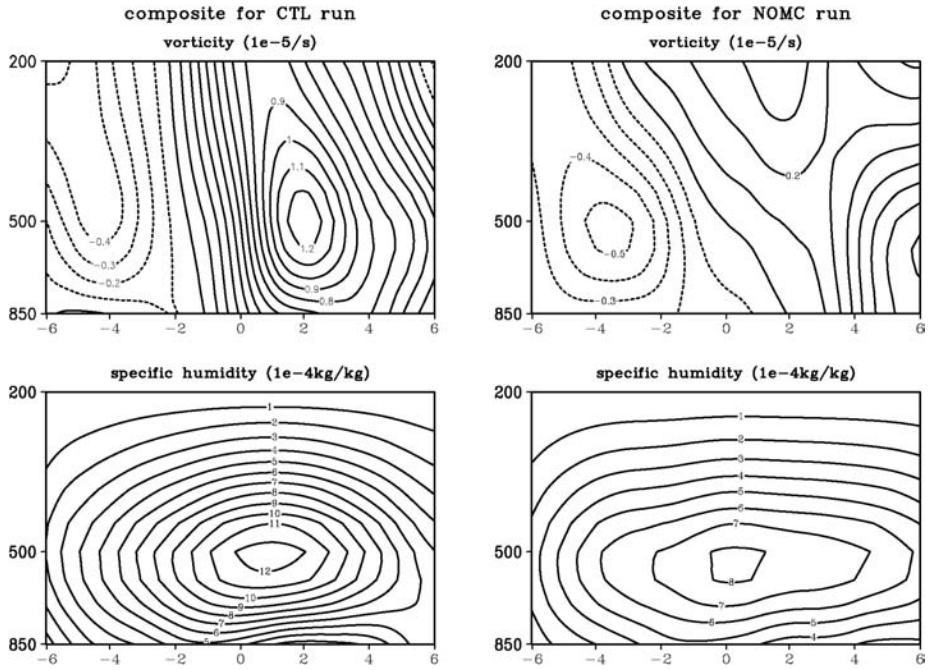

Fig. 5. Meridional-vertical structures of the composite northward propagating boreal summer intraseasonal oscillation BSISO relative vorticity (10^{-5} s^{-1}, top panels) and specific humidity (10^{-4} kg kg^{-1}, bottom panels) fields from the control CTL experiment (left panels) and the no-Maritime Continent NOMC experiment (right panels). The composite is based on the strong northward-propagating ISO events along 65°–160°E. Horizontal axis is the meridional distance (unit: 1° lat) relative to the ISO convection center, with a positive (negative) value being north (south) of the convection center. The vertical axis is the pressure (hPa).

tion of the background easterly vertical shear due to the removal of the Maritime Continent accounts for the weakening of the asymmetric positive vorticity north of the convection center, which in turn causes the reduction of the northward propagating variance over the monsoon sector.

The meridional-vertical structure of the composite ISO moisture field shows a maximum low-level specific humidity center about 100 km (50 km) north of the convection center in the CTL (NOMC) experiment (bottom panels in Fig. 5), similar to the observation (Jiang et al. 2004). However, the intensity of the asymmetric moisture is greater in the CTL than that in the NOMC experiment. The difference in the moisture asymmetry may also contribute to the changes in the northward propagation variance.

To reveal the cause of the difference in the moisture asymmetry, we examine the perturbation moisture advection by the background southerly and by the mean meridional humidity gradient. As discussed in Jiang et al. (2004) (see their schematic diagrams Figs. 12 and 14), the advection effect by the mean meridional wind in the boundary layer may shift the specific humidity perturbation to the north of the convection (i.e., $\frac{\partial q}{\partial t} \propto -\bar{v}_B \frac{\partial q}{\partial y}$), while the advection effect by the perturbation wind and the mean meridional humidity gradient may also shift the humidity center to the north (i.e., $\frac{\partial q}{\partial t} \propto -v_B \frac{\partial \bar{q}}{\partial y}$). The model background low-level flow and meridional humidity gradient are shown in Figs. 6b and 6c. Note that there is a significant reduction of the background low-level southerly and meridional humidity gradient in the NOMC experiment, both of which may reduce the moisture asymmetry due to the weakening of the perturbation moisture advection.

What causes the background mean flow (including vertical shear) and moisture changes? As shown in Fig. 8, removing the Maritime Continent leads to the increase of the surface moisture and thus enhanced (reduced) convection in the equatorial region (at 15°–20°N) over the Maritime Continent longitudes. In CTL, the local Hadley circulation favors a strong ascending branch over the monsoon trough latitudes (15°–20°N) and a weak subsi-

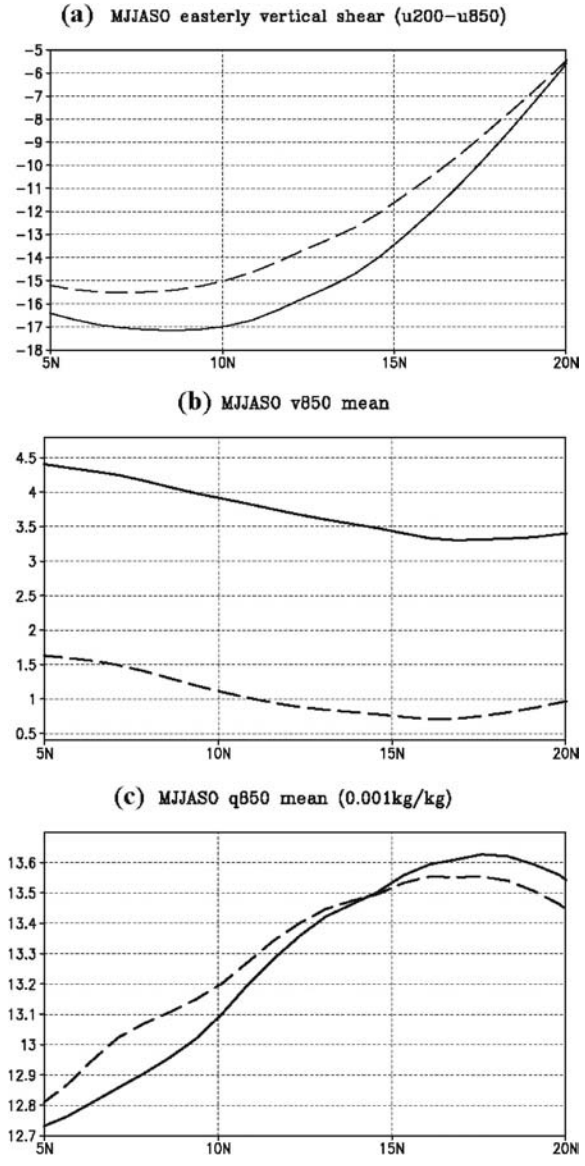

Fig. 6 Meridional distributions of the background vertical shear (a), 850-hPa meridional wind (b) and 850-hPa specific humidity (c) fields averaged over 65°–160°E during May to October MJJASO in the control CTL (solid line) and no-Maritime Continent NOMC (dashed line) experiments.

dence branch over the southern Maritime Continent. Removing the Maritime Continent leads to the weakening of this meridional overturning circulation and thus the decrease of the low-level southerly (Fig. 6b). The reduced northward wind further weakens northward moisture transport and thus the mean meridional humidity gradient (Fig. 6c). The weakening of the monsoon trough heating leads to the decrease of the easterly shear over the region according to the thermal wind relation (Fig. 6a).

To further illustrate the difference in the northward propagation between CTL and NOMC, we examine the composite evolution of the ISO rainfall anomaly (mm day^{-1}) from day −10 to day 12 in both the CTL and NOMC experiments (Fig. 7). Shading in the figure represents a positive rainfall anomaly larger than 3 mm day^{-1} associated with ISO. Day 0 represents a reference time when the ISO rainfall anomaly center moves to 110°E along 5°S–5°N. Unlike the CTL experiment in which more BSISO convective events bifurcate northward before reaching the Maritime Continent (Fig. 7a), the BSISO convection in NOMC continues to move eastward across the Maritime Continent (Fig. 7b). The composite maps present a clear evidence of stronger (weaker) northward propagation in the CTL (NOMC) experiment.

4.2 Eastward propagation

The examination of variance of the eastward propagation reveals that a maximum increase of the variance appears over the Maritime Continent longitudes in the NOMC experiment (Fig. 2). The overall strength of the eastward propagation is strengthened in NOMC (Fig. 3), although the difference just exceeds the 90% confidence level.

The increase of the eastward propagation variance is possibly attributed to the increase of the mean convection over the Maritime Continent (Fig. 8). In the observation and CTL, a northward shift of the thermal equator leads to maximum convection at 15°–20°N and weak subsidence at and south of the equator over the Maritime Continent longitudes. This equatorially asymmetric mean condition does not favor the growth of the equatorial Kelvin wave and therefore the Rossby waves are emanated from the decaying equatorial Kelvin-Rossby wave couplet (Wang and Li 1994; Li and Wang 1994; Wang and Xie 1997). The increase of the surface moisture over the Maritime Continent in the NOMC experiment enhances the local convection and leads to the reduced asymmetry of the local meridional circulation (Fig. 8), which is argued to help maintain the equatorial coupled Kelvin-Rossby wave couplet. This may be a reason to enhance the overall variance of the eastward propagation.

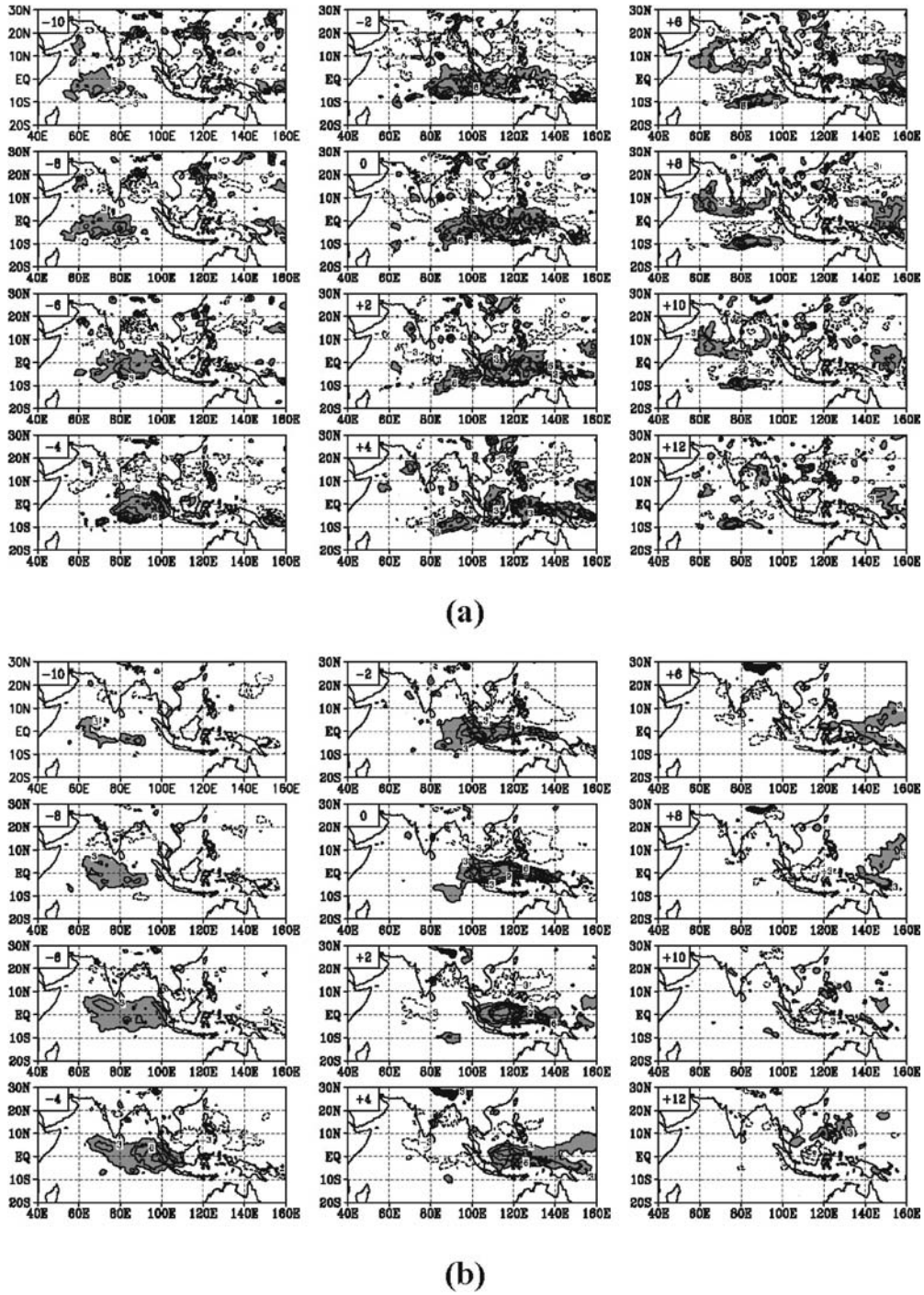

Fig. 7. Composite evolution of the intraseasonal oscillation ISO rainfall anomaly (mm day^{-1}) from day −10 to day 12 for (a) the control CTL experiment (top) and (b) the no-Maritime Continent NOMC experiment (bottom). Shading indicates the area of a positive rainfall anomaly larger than 3 mm day^{-1}. Day 0 represents a reference time when the ISO rainfall center moves to 110°E along 5°S–5°N.

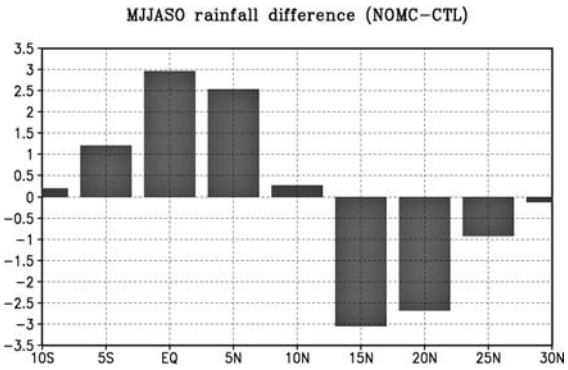

Fig. 8. The difference of May to October MJJASO rainfall rates (mm day^{-1}) between the no-Maritime Continent NOMC and control CTL experiments (NOMC–CTL) averaged over the Maritime Continent longitudes (100°–160°E).

Slingo et al. (2003) suggested a possible role of the diurnal cycle in altering the ISO variance over the Maritime Continent. The argument is that the local diurnal cycle over the Maritime Continent may compete for moisture sources with the ISO. This motivates us to examine the change of strength of the diurnal cycle due to the absence of the Maritime Continent. Figure 9 shows the MJJASO mean diurnal range of rain rates derived from the CTL and NOMC experiment, respectively. The diurnal range is defined as climatological daily maximum precipitation minus daily minimum precipitation, as described by Kikuchi and Wang (2008). It is shown that removing the Maritime Continent leads to a great weakening of the diurnal cycle over the Maritime Continent region. The area-averaged strength is 3–4 times smaller. This implies that the weakening of the local diurnal

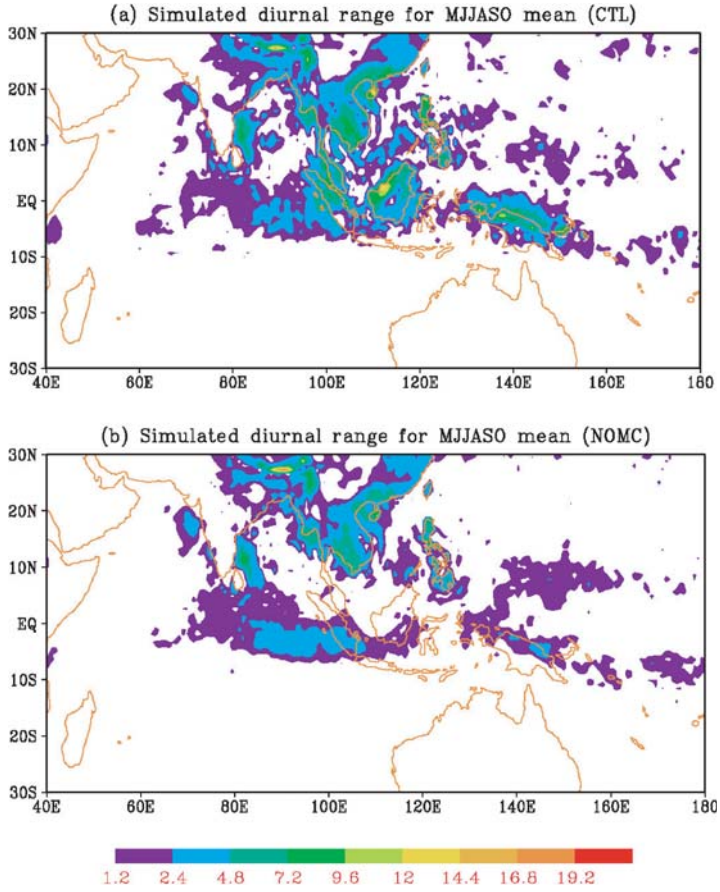

Fig. 9. The averaged diurnal range of rain rates (mm day^{-1}) in May to October MJJASO derived from the control CTL experiment (a) and no-Maritime Continent NOMC experiment (b), respectively. The diurnal range is defined as the climatological daily maximum minus minimum precipitation.

cycle is another possible factor that enhances the eastward propagation and overall ISO variances over the Maritime Continent, in addition to increased surface moisture and decreased surface roughness, in the NOMC experiment.

5. Summary and discussion

The influence of the Maritime Continent on the BSISO propagation characteristics was investigated on the basis of the diagnosis of two high-resolution (T159L31) ECHAM5.3 AGCM simulations with and without the presence of the Maritime Continent in the model lower boundary condition. The most notable changes, as revealed by a finite domain WFS analysis, are the enhancement of the eastward propagation along the equator and the weakening of the northward propagation over the entire monsoon region (65°–160°E) while the Maritime Continent is removed. A student T or t test indicates that the difference of the northward propagation between the CTL and NOMC experiments exceeds the 95% confidence level, whereas the difference of the eastward propagation just exceeds the 90% confidence level.

The composite BSISO evolution patterns show that, in both the simulations, the BSISO is originated in the equatorial western Indian Ocean. In CTL, with the presence of the Maritime Continent, there is an evidence of northward bifurcation or the Rossby wave emanation before the ISO convection reaches the Maritime Continent (Fig. 7a). The northward propagation is significantly reduced when the Maritime Continent is removed (Fig. 7b).

The diagnosis of the meridional-vertical structure of the northward-propagating BSISO modes in both the simulations reveals a difference in the meridional asymmetry of the vorticity and specific humidity fields with respect to the ISO convection center. A weakened meridional asymmetry of the vorticity and humidity appears in the NOMC case. A significant weakening of the vorticity and moisture asymmetries accounts for the decrease of the northward propagation variance.

The cause of the weakening of the meridional asymmetry is possibly attributed to the change of the background vertical wind shear, low-level southerly, and north-south moisture gradient. According to the vertical shear mechanism, the monsoon easterly shear, through its interaction with the ISO convection, leads to the northward shift of the vorticity. The decrease of the mean easterly shear between 5°N and 20°N in the NOMC experiment thus leads to the weakening of the vorticity asymmetry. The reduction of the moisture asymmetry in the NOMC experiment is attributed to the reduced moisture advection, owing to the weakening of both the mean low-level southerly and the mean meridional humidity gradient.

The diagnosis of the model mean state reveals that removing the Maritime Continent leads to the increases of the local surface humidity and thus equatorial convection over the Maritime Continent longitudes. This may favor the growth and development of the equatorial Kelvin-Rossby wave couplet and thus enhance the eastward propagation along the equator. The enhanced equatorial convection also leads to a weakened local Hadley circulation, which, on one hand, decreases the mean low-level southerly and the mean meridional moisture gradient (due to reduced northward moisture transport) and, on the other hand, weakens the monsoon trough heating and thus the background easterly shear.

It is worth mentioning that the maximum difference of the northward propagation spectrum between the CTL and NOMC experiments appears at 20–30 days while the maximum spectrum in CTL is around 25–50 days. Thus the spectrum peak of the BSISO in the NOMC run is slightly shifted compared to the CTL run (Fig. 4). The similar spectrum distribution between the NOMC simulation and the observation implies that the model has a systematic bias in the simulation of ISO variability. Thus, a caution is needed when one interprets the model simulation results. The physical interpretation of change of the ISO propagation characteristics in the sensitivity experiment is qualitative and requires a further quantitative diagnosis support. In the current study, AGCM-only experiments were conducted. It is anticipated that removal of the Maritime Continent in a completely coupled atmosphere-ocean model will result in a marked change in the warm pool location and the tropical mean atmospheric and oceanic states in general.

The high-resolution AGCM simulations, for the first time, showed a significant impact of the Maritime Continent on the BSISO propagation characteristics through the change of the diurnal cycle, surface moisture and local Hadley circulation. The result may help us to better understand the mechanisms related to the BSISO propagation. A subsequent study will be an investigation of the mean flow effect on the equatorial Kelvin and Rossby

wave dynamics. An eigenvalue analysis of such a mean flow effect is currently ongoing, and the result will be reported elsewhere.

Acknowledgments

This work was supported by ONR/NRL grants N000140810256 and N00173-09-1-G008, by the International Pacific Research Center that is sponsored by the Japan Agency for Marine-Earth Science and Technology (JAMSTEC), NASA (NNX07AG53G) and NOAA (NA17RJ1230), and by the Special Funds for Public Welfare of China [Grant No. GYHY(QX) 2008-06-005]. This is SOEST contribution number 7905 and IPRC contribution number 681.

References

Chen, T.-C., and M. Murakami, 1988: The 30–50 day variation of convective activity over the western Pacific Ocean with the emphasis on the northwestern region. *Mon. Wea. Rev.*, **116**, 892–906.

Fu, X., B. Wang, T. Li, and J. P. McCreary, 2003: Coupling between northward propagating, intraseasonal oscillations and sea-surface temperature in the Indian Ocean. *J. Atmos. Sci.*, **60**, 1733–1753.

Hayashi, Y., 1982: Space–time spectral analysis and its applications to atmospheric waves. *J. Meteor. Soc. Japan*, **60**, 56–171.

Hsu, H.-H., B. J. Hoskins, and F.-F. Jin, 1990: The 1985/86 intraseasonal oscillation and the role of the extratropics. *J. Atmos. Sci.*, **47**, 823–839.

Inness, P. M., and J. M. Slingo, 2006: The interaction of Madden-Julian Oscillation with the Maritime Continent in a GCM. *Quart J. Royal Meteor. Soc.*, **132**, 1645–1667.

Jiang, X., T. Li, and B. Wang, 2004: Structures and mechanisms of the northward propagating boreal summer intraseasonal oscillation. *J. Climate*, **17**, 1022–1039.

Jiang, X., and T. Li, 2005: Re-initiation of the boreal summer intraseasonal oscillation in the tropical Indian Ocean. *J. Climate*, **18**, 3777–3795.

Kikuchi, K., and B. Wang, 2008: Diurnal precipitation regimes in the global Tropics. *J. Climate*, **21**, 2680–2696.

Krishnamurti, T. N., and D. Subrahmanyam, 1982: The 30–50 day mode at 850mb during MONEX. *J. Atmos. Sci.*, **39**, 2088–2095.

Lau, K.-M., and L. Peng, 1987: Origin of low frequency (intraseasonal) oscillation in the tropical atmosphere, Part I: The basic theory. *J. Atmos. Sci.*, **44**, 950–972.

Li, T., F. Tam, X. Fu, T. Zhou, and W. Zhu, 2008: Causes of the Intraseasonal SST Variability in the Tropical Indian Ocean, *Atmosphere-Ocean Science Letters*, **1**, 18–23.

Li, T., and B. Wang, 1994: The influence of sea surface temperature on the tropical intraseasonal oscillation: a numerical study. *Mon. Wea. Rev.*, **122**, 2349–2362.

Li, T., and C. Zhou, 2009: Planetary scale selection of the Madden-Julian Oscillation. *J. Atmos. Sci.*, **66**, 2429–2443.

Liess, S., D. E. Waliser, and S. D. Schubert, 2005: Predictability Studies of the Intraseasonal Oscillation with the ECHAM5 GCM. *J. Atmos Sci.*, **62**, 3320–3336.

Lin, X., and R. H. Johnson, 1996: Kinematic and thermodynamic characteristics of the flow over the western Pacific warm pool during TOGA COARE. *J. Atmos. Sci.*, **53**, 695–715.

Lin A.-L., and T. Li, 2008: Energy Spectrum Characteristics of Boreal Summer Intraseasonal Oscillations: Climatology and Variations during the ENSO Developing and Decaying Phases. *J. Climate*, **21**, 6304–6320.

Madden, R. A., and P. R. Julian, 1971: Detection of a 40–50 day oscillation in the zonal wind in the tropical Pacific. *J. Atmos. Sci.*, **28**, 702–708.

Madden, R. A., and P. R. Julian, 1972: Description of global-scale circulation cells in the Tropics with a 40–50 day period. *J. Atmos. Sci.*, **29**, 3138–3158.

Maloney, E. D., and A. H. Sobel, 2004: Surface Fluxes and Ocean Coupling in the Tropical Intraseasonal Oscillation. *J. Climate*, **17**, 4368–4386.

Matthews, A. J., 2008: Primary and successive events in the Madden-Julian oscillation. *Quart J. Roy. Meteor. Soc.*, **134**, 439–453.

Neale, R., and J. Slingo, 2003: The Maritime Continent and its role in the global climate: A GCM study. *J. Climate*, **16**, 834–848.

Nordeng, T. E., 1994: Extended versions of the convective parameterization scheme at ECMWF and their impact on the mean and transient activity of the model in the tropics. *Tech. Memor.*, **206**, Eur. Cent. for Medium-Range Weather Forecasts, Reading, U. K.

Pan, L., and T. Li, 2007: Interactions between the tropical ISO and mid-latitude low-frequency flow. *Clim. Dyn.*, **31**, 375–388.

Roeckner, E., and Coauthors, 2003: The atmospheric general circulation model ECHAM5. Part I: Model description. *Max-Planck-Institut für Meteorologie Rep.* **349**, Hamburg, Germany, 140 pp.

Rui, H., and B. Wang, 1990: Development characteristics and dynamic structure of tropical intraseasonal convection anomalies. *J. Atmos. Sci.*, **47**, 357–379.

Salby, M. L., and H. H. Hendon, 1994: Intraseasonal behavior of clouds, temperature, and motion in the tropics. *J. Atmos. Sci.*, **51**, 2207–2224.

Slingo, J., P. Inness, R. Neale, S. Woolnough, and G.-Y., Yang, 2003: Scale interactions on diurnal to seasonal timescales and their relevance to model systematic errors. *Annals Geophys.*, **46**, 139–155.

Teng, H., and B. Wang, 2003: Interannual variations of the boreal summer intraseasonal oscillation in the Asian-Pacific region. *J. Climate*, **16**, 3572–3584.

Tiedtke, M., 1989: A comprehensive mass flux scheme for cumulus parameterization in largescale models. *Mon. Wea. Rev.*, **117**, 1779–1800.

Tompkins, A. M., 2002: A prognostic parameterization for the subgrid-scale variability of water vapor and clouds in large-scale models and its use to diagnose cloud cover. *J. Atmos. Sci.*, **59**, 1917–1942.

Wang, B., and T. Li, 1994: Convective interaction with boundary-layer dynamics in the development of a tropical intraseasonal oscillation. *J. Atmos. Sci.*, **51**, 1386–1400.

Wang, B., and X. Xie, 1997: A model for the boreal summer intraseasonal oscillation. *J. Atmos. Sci.*, **54**, 72–86.

Webster, P. J., 1983: Mechanisms of low-frequency variability: Surface hydrological effects. *J. Atmos. Sci.*, **40**, 2110–2124.

Xie, P., and P. A. Arkin (1997), Global precipitation: A 17-year monthly analysis based on gauge observations, satellite estimates and numerical model outputs, *Bull. Amer. Meteor. Soc.*, **78**, 2539–2558.

Yasunari, T., 1979: Cloudiness fluctuations associated with the Northern Hemisphere summer monsoon. *J. Meteor. Soc. Japan*, **57**, 227–242.

Zhang, C. D., and H. H. Hendon, 1997: Propagating and standing components of the intraseasonal oscillation in tropical convection. *J. Atmos. Sci.*, **54**, 741–752.